siGOLD: a Serial Multiplex Immunogold Labeling Method for Identifying Peptidergic Neurons in Connectomes

Réza Shahidi[1], Elizabeth Williams[1], Markus Conzelmann[1], Albina Asadulina[1], Csaba Verasztó, Sanja Jasek[1], Luis A. Bezares-Calderón[1] and Gáspár Jékely[1*]

[1]Max-Planck-Institute for Developmental Biology, Spemannstraße. 35, Tübingen D- 72076, Germany

[*]Corresponding author
Email: gaspar.jekely@tuebingen.mpg.de

ABSTRACT

Connectomics aims to comprehensively map synaptic connections in blocks of neural tissue. However, current approaches are limited in directly assigning molecular identities to neurons in a connectome. Here, we use serial multiplex immunogold labeling (siGOLD) combined with serial-section transmission electron microscopy (ssTEM) to reveal the identity of multiple peptidergic neurons in a connectome. The unique antigenicity of neuropeptides, combined with their uniform distribution along axons, allowed us to identify distinct neurons by immunolabeling a small subset of sections within larger series. We demonstrate the scalability of siGOLD by identifying several peptidergic neurons using 11 neuropeptide antibodies on a full-body larval ssTEM dataset of the annelid *Platynereis*. We also reconstruct the circuitry of the sensory nuchal organs that were found by siGOLD to express the circadian neuropeptide pigment-dispersing factor. Our approach opens up the possibility for directly overlaying chemical neuromodulatory maps onto synaptic connectomic maps in the study of nervous systems.

INTRODUCTION

A comprehensive understanding of nervous system function requires knowledge of not only the precise connectivity of neurons but also of the unique combinations of molecules expressed by each neuron. Connectomics uses serial-sectioning electron microscopy (EM) to map the synapse-level connectivity of entire neural circuits (Morgan and Lichtman, 2013). However, connectomes provide an incomplete picture of the nervous system, since they lack information about the molecular nature of neurons. In particular, neuromodulators are known to actively shape the output of circuits by modifying synaptic function and neuron excitability (Bargmann, 2012; Bargmann and Marder, 2013; Bucher and Marder, 2013; Marder, 2012). The direct mapping of the source of neuromodulators onto synapse-level anatomical maps would help integrate the connectomic and neuromodulatory perspectives and enrich our understanding of circuit function.
To assign molecular identities to neurons on EM sections, several approaches have been developed. Genetically encoded tags with enzymatic activity, such as miniSOG and APEX probes, allow the resolution of cells or subcellular structures by EM following incubation with a substrate that is converted to electron-dense deposits (Martell et al., 2012; Shu et al., 2011). Fixation resistant protein tags compatible with EM procedures and observable by correlative light and electron microscopy (CLEM) or directly by immunogold labeling (immunoEM) have also been developed, such as the smGFPs (Viswanathan et al., 2015). However, these probes must be expressed in specific neurons using transgenesis, limiting their use to one or a few cell types, such as in the "two-tag" labeling approach (Lin et al., 2015).

An alternative approach is the use of endogenous targets, as in array tomography, a method that combines sequential immunofluorescence (IF) with several different antibodies to obtain molecular information and EM to resolve ultrastructural detail (Collman et al., 2015; Micheva and Smith, 2007). However, the sequentially acquired IF and EM images need to be registered. Array tomography also relies on embedding the specimen in porous, hydrophilic acrylic resins to allow optimal immunolabeling. For large-scale serial sectioning projects, epoxy resins, such as Epon, are favored due to their higher stability during sectioning and imaging and the optimal ultrastructural preservation they provide (Bock et al., 2011; Briggman et al., 2011; Bumbarger et al., 2013; Ohyama et al., 2015; Randel et al., 2015; White et al., 1986). However, the Epon-embedding procedure, including osmium-fixation and resin polymerization at 60 °C, compromises the immunogenicity of endogenous targets (Brorson, 1998; Brorson and Reinholt, 2008; De Paul et al., 2012). Current immunolabeling approaches therefore sacrifice the mechanical stability and ultrastructural contrast of the sample for optimal gold labeling.
Here, we introduce siGOLD or serial-multiplex immunogold, a method for immunolabeling connectomes. We found that amidated neuropeptide epitopes show exceptional and long-term immunopreservation in Epon-embedded samples, allowing us to simultaneously obtain high ultrastructural detail and specific immunogold signal. Since neuropeptides occur throughout the axon of peptidergic neurons (Wong et al., 2012; Zupanc, 1996), immunolabeling of only a few sections with neuropeptide antibodies was sufficient to identify peptidergic neurons. Using siGOLD with 11 distinct antibodies on the same specimen, we identified several neuropeptide-containing neurons in the larval connectome of the marine annelid *Platynereis dumerilii*, a model for circuit neuroscience (Randel et al., 2014; Randel et al., 2015; Tosches et al., 2014). By combining siGOLD with whole-body circuit reconstructions, we could assign molecular identities to different neurons and analyze their connectivity at EM resolution.

RESULTS

Multiplex neuron identification with siGOLD on serial sections

In order to selectively label individual neurons in large-scale serial EM datasets, we established an immunoEM procedure to label ultrathin sections with neuronal cell-type specific antibodies. We reasoned that immunoEM performed on only a few layers from a large series of sections could identify neuron profiles that contain the antigen (Figure 1A, B). We first performed immunoEM on 40-nm serial sections cut from the ventral nerve cord (VNC) of a 72 hr post-fertilization (hpf) *Platynereis* larva (specimen HT9-5). For specimen preparation, we used a conventional serial TEM protocol including high-pressure freezing, fixation with a freeze substitution medium containing 2% osmium tetroxide and 0.5% uranyl acetate, and embedding in Epon. We also developed a procedure for the safe handling of several grids in parallel during the immunostaining and contrasting procedure. We optimized the immunolabeling protocol to achieve high specificity for immunoEM and high ultrastructural detail. In our protocol, we use ultra small gold-coupled secondary antibodies and a silver-enhancement procedure. We also fine-tuned the contrast-staining protocol to optimize contrast for both gold labeling and ultrastructural detail.

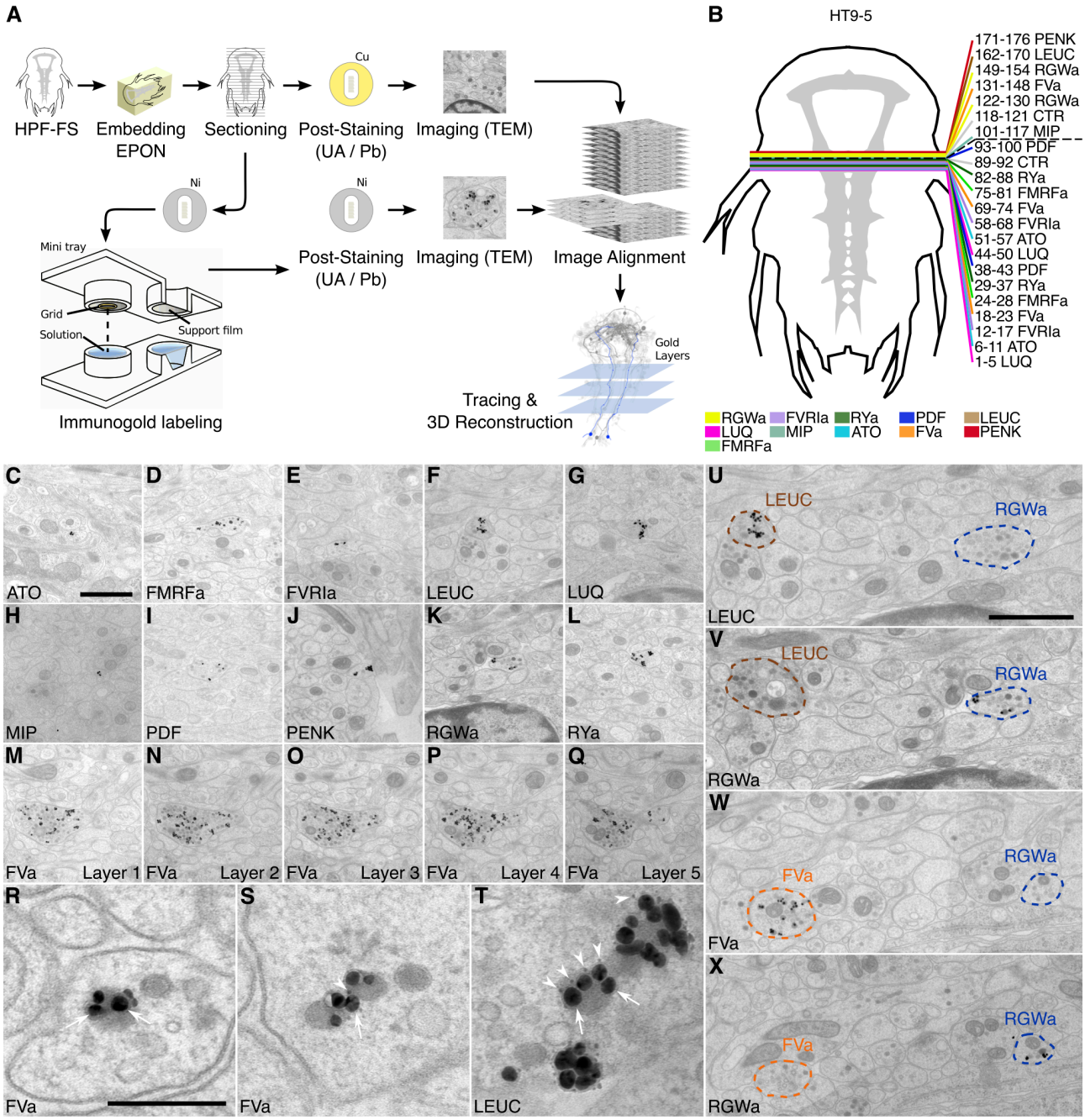

Figure 1. Development of the siGOLD method
(A) Schematic flowchart of the siGOLD labeling approach from high-pressure freezing and freeze substitution (HPF-FS) to tracing and 3D reconstruction. Ni, nickel grid, Cu, copper grid. (B) Schematic of the HT9-5 sample showing the position of the ventral nerve cord (VNC), ventral view. Colored lines indicate where cross-sections through the VNC were taken, near the base of the circumesophageal connective at the first commissure. Layer number(s) followed by neuropeptide ID is indicated for each colored line. Dashed line indicates the gap (missing sections) between the first and second series of sections. (C-Q) Representative micrographs with immunogold labeled axons for the neuropeptide antibodies indicated. (M-Q) Series of five adjacent sections labeled with FVa neuropeptide antibody (FVa 1-5). (R-T) High-resolution micrographs of immunogold labeled, silver-enhanced gold particles (arrows), and unenhanced ultra small gold particles (arrowheads) (U-X) Neurite-specific labeling in adjacent sections (7 sections apart) labeled with different antibodies. Scale bar: (C-Q) 1 µm; (R-T) 200 nm; (U-X) 1 µm.

We decided to test neuropeptide antibodies as cell-specific neuronal markers because neuropeptides are concentrated in vesicles and neuropeptide-containing vesicles are distributed throughout the axon of peptidergic neurons. Neuropeptides are also often chemically modified, including C-terminal amidation (Eipper et al., 1992), which confers stability and high immunogenicity to even

very short peptides (Conzelmann and Jékely, 2012). In preliminary tests, we found strong and localized labeling in neurites using 11 different polyclonal antibodies generated against short amidated neuropeptides of *Platynereis* (Table 1).

NP precursor name	**Abbreviation**	**Antigen**
FMRFamide	FMRFa	(C)FMRFa
RYamide	RYa	(C)VFRYa
Myoinhibitory peptide/Allatostatin B	MIP	(C)AWNKNSMRVWa or (C)VWa
RGWamide	RGWa	(C)RGWa or (C)GWa
Proenkephalin	PENK	(C)YGDLSFSNSNYa
Luqin	LUQ	(C)WRPQGRFa
Allatotropin	ATO	(C)GFRTGAYDRFSHGFa
Pigment dispersing factor	PDF	(C)NPGTLDAVLDMPDLMSLa
leucokinin	LEUC	(C)KFTPWAa
FVamide	FVa	(C)AHRFVa or (C)FVa
FVRIamide	FVRIa	(C)FVRIa

Table 1. List of antibodies used
The full name and abbreviation of neuropeptide precursors that contain the neuropeptides used for immunization. All 11 neuropeptides are amidated (a). A Cys (C) was added to the N-terminus of each peptide to allow coupling during immunization and affinity purification.

To test the specificity and reproducibility of immunoEM with the 11 neuropeptide-antibodies, we collected two sets of transverse serial sections from the 1st trunk segment of the HT9-5 specimen. 4 to 18 consecutive serial sections were collected on each EM grid for immunoEM. For each antibody, we stained two grids separated by a serial distance of approximately 50 sections (Figure 1B). We imaged the VNC region in each section at high resolution (2.22 nm/pixel) followed by stitching and alignment of the images. We found strong and localized labeling in only a small subset of neurites for each antibody (Figure 1C-L). In consecutive sections, the same neurite was often strongly labeled with the same antibody (Figure 1M-Q). In sections collected on different grids that were labeled with different antibodies, we found distinct patterns of neurite-specific labeling (Figure 1U-X). In many sections, we could observe dense core vesicles in the cytoplasm of the gold-labeled neurites, indicative of the peptidergic nature of these cells (Figure 1C-Q). In high-resolution (0.22 nm/pixel) images we could observe gold labeling associated with dense core vesicles (Figure 1R-T), suggesting that our immunoEM procedure labeled mature neuropeptides residing inside these vesicles.
Next, we scored the distribution of gold particles in the VNC series (Figure 2). We selected all neurites that were labeled with two or more gold particles in any of the immunoEM sections and traced these neurites across all sections. We also selected 50 control neurites along a coronal transect spanning the VNC and traced these across all sections (Figure 2A). We then counted all gold particles in each traced neurite and tabulated the results. The gold particles were also summed for each antibody to show a concise summary of all gold labels (Figure 2B and D). Since in the high-resolution images we also observed several ultra-small gold particles that were not enhanced during silver-enhancement, our comprehensive gold counts performed on lower-resolution images likely underestimate the intensity of gold labeling (Figure 1R-T).

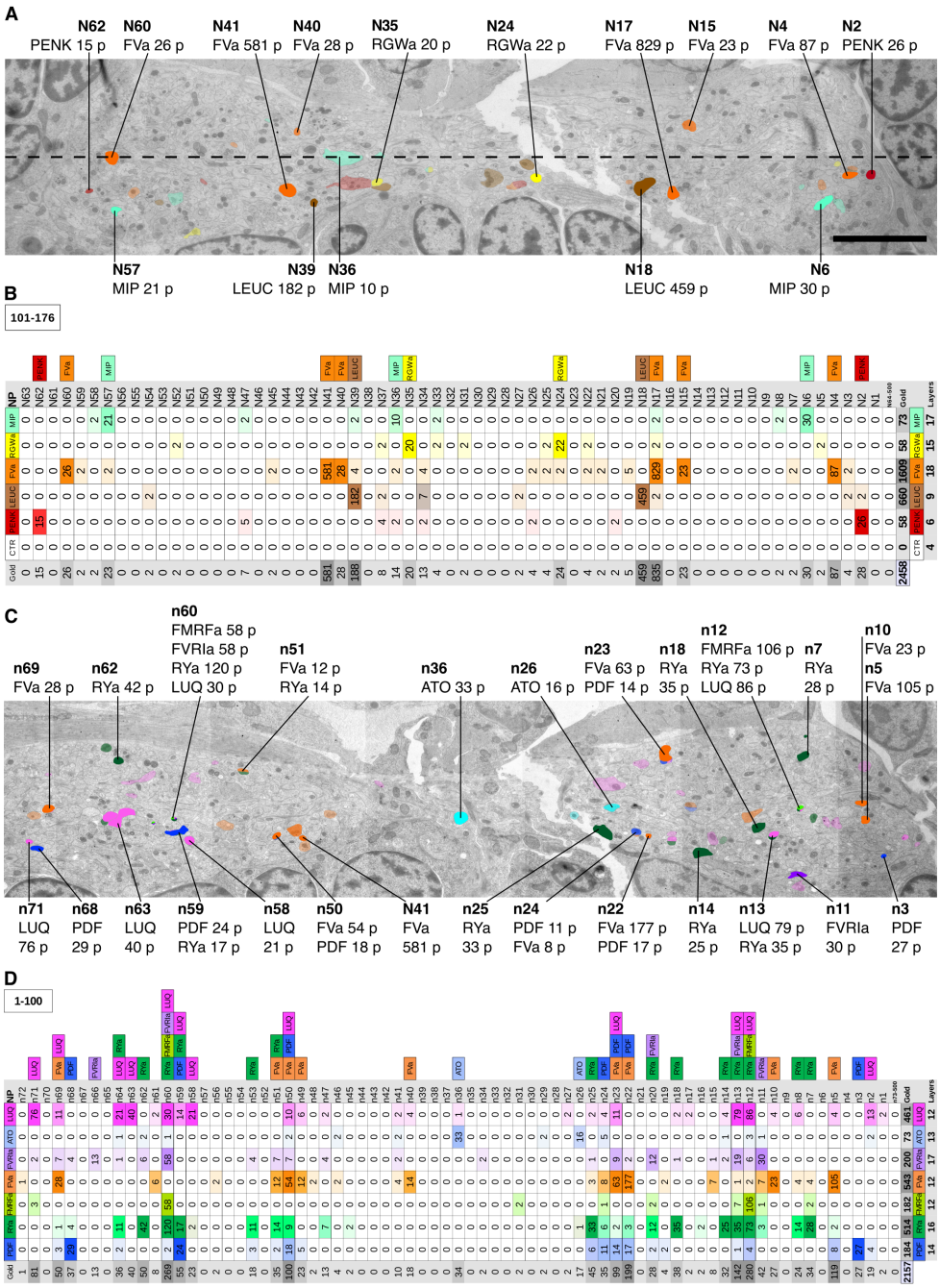

Figure 2. Identification of peptidergic neurites by siGOLD in a 72 hpf *Platynereis* specimen
(A, C) Apical view of EM cross-section through the VNC near the first commissure. Dorsal side of larva is to the top. Strongly labeled neurites were analyzed across the whole VNC region. Control axon profiles were analyzed along a transect (dotted line). Two axon profiles were sampled every 1 µm. Totals of 72 and 63 axons were examined for the first and second series of sections respectively (an approximately 10-section gap occurs between the two series). Colored cell profiles indicate gold labeled neuropeptidergic axons. Different shades of a color represent an approximation of labeling intensity; the lighter the shade, the lower the intensity. Positive axons are tagged with neuron number, neuropeptide name, and total number of gold particles per total number of layers for that neuropeptide. (B, D) Tables show number of gold particles per axon for each neuropeptide. All strongly labeled axons across the VNC and control axons along the sampled transect are shown. Data were arranged according to the spatial distribution of the corresponding neurites in the VNC. Each sampled axon was traced across all layers and counted for its total number of gold particles. Columns indicate neurons and an ID with 'n' is given to each neuron in the first series of sections and 'N' for neurons in the second series of sections. Rows indicate neuropeptide immunogold labels. Different shades of the same color indicate intensity of gold labeling. A cut-off value of 10 gold particles per axon was chosen to only highlight strongly labeled profiles. Totals are shown for each row (neuropeptide) and each column (axon profile). In the final column of each table, the total number of layers stained for each neuropeptide is shown. Scale bar: 5 µm.

Our quantifications revealed a high neurite-specificity of immunogold labeling with all 11 neuropeptide antibodies (Figure 2). The VNC in our sample contained approximately 1600 neurite cross-sections and the majority of these showed no gold labeling. However, for each antibody we could identify a small number of neurites that consistently showed strong labeling across different sections (Figure 2). Neurites that were labeled on one grid were also strongly labeled on their grid pair with the same antibody separated by approximately 50 sections. The pattern of the labeled neurites also showed bilateral symmetry, further supporting the labeling of specific peptidergic neuron populations in the bilaterally symmetrical VNC. In sections where we omitted the primary antibody, we did not see any gold labeling in any of the traced neurites (Figure 2B).
The siGOLD approach also allowed us to detect the coexpression of some neuropeptides in the same neurons. For example, we found coexpression of FVa and PDF neuropeptides in a subset of the neurites labeled by these two antibodies (Figure 2D). Some antibodies showed extensive overlap in labeling, including the FMRFa, luqin and the RYa antibodies.
To test if the antibodies specifically recognize the neuropeptides we used for immunization, we performed morpholino-mediated knockdown experiments of proneuropeptide expression. The specificity of the MIP antibody was demonstrated previously (Williams et al., 2015). We performed microinjections with 10 different translation-blocking morpholinos, one targeting each remaining proneuropeptide. We then performed triple IF using an acetylated tubulin antibody, a rat FVa antibody, and the respective rabbit neuropeptide antibodies. The acetylated tubulin antibody allowed us to exclude developmental abnormalities caused by morpholino injection. The rat FVa antibody provided a further control to exclude that morpholino injection affected proneuropeptide processing in general. For eight out of 10 antibodies (FVa, FMRFa, ATO, FVRIa, PDF, RGWa, PENK, LEUC), morpholino injection strongly reduced IF signal with the respective antibody (Supplementary figure 1). For the FMRFa antibody, we did not detect staining in the VNC following morpholino injection, but we could still detect staining in the head. The FMRFa antibody therefore likely recognizes other antigens, such as other RFa peptides in the head. For the RYa and LUQ antibodies, we did not see a reduction in staining intensity in the VNC following morpholino injection. These two morpholinos may not have knocked down proneuropeptide expression efficiently or the antibodies may cross-react with other RFamide peptides. A cross reactivity of antibodies raised against R[Y|F]amide peptides was also suggested by the labeling of an overlapping set of neurites with the FMRFa, LUQ, and RYa antibodies by siGOLD (Figure 2). Without knowing the exact antigen specificity for these antibodies, we can nevertheless use them as specific markers of R[Y|F]amidergic axons.

Comparison of siGOLD labeling to whole-mount immunofluorescence

siGOLD labeling of consecutive sections with 11 antibodies revealed the arrangement of several peptidergic neurites in the VNC (Figure 2). To test if this spatial arrangement is consistent between siGOLD and IF labeling of whole specimens we analyzed the labeling with all 11 antibodies in whole-mount *Platynereis* 72 hpf larval samples. All antibodies labeled subsets of longitudinal axons spanning the entire length of the VNC and occurring in different mediolateral positions (Figure 3).

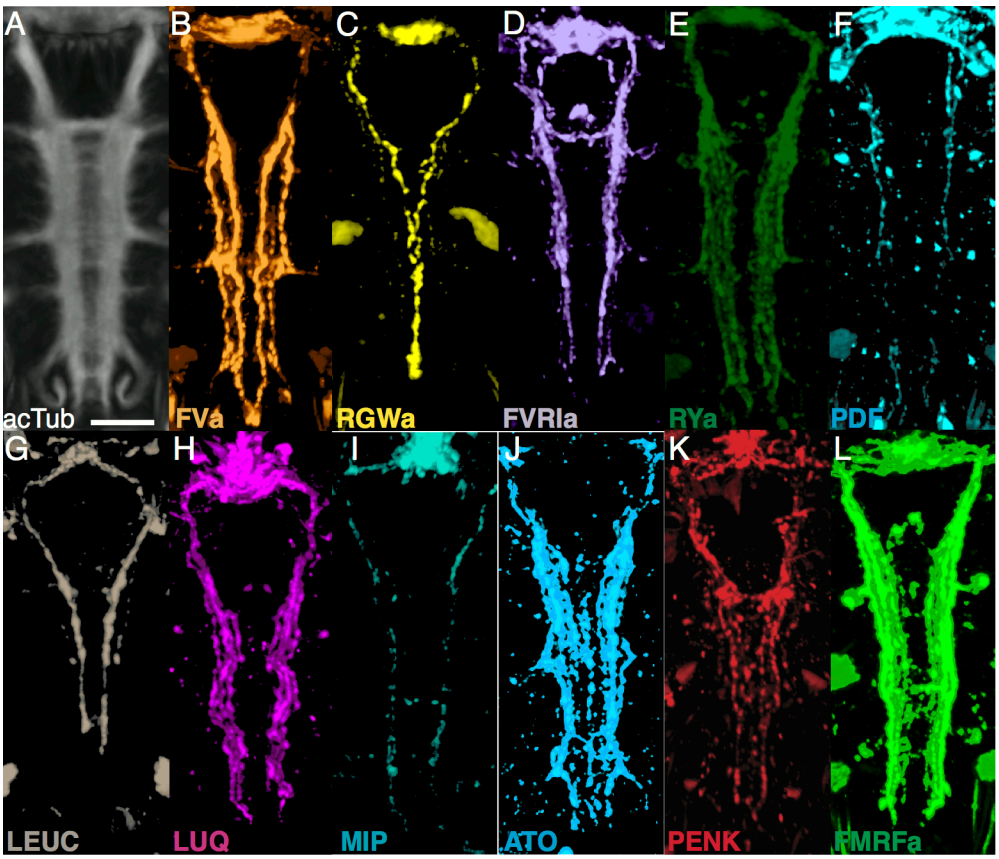

Figure 3. Whole-mount IF of *Platynereis* larvae with antibodies raised against neuropeptides labels distinct subsets of neuronal tracks in the VNC. (A) Ventral view of *Platynereis* VNC, stained with an antibody raised against acetylated tubulin. This is the registered average VNC generated from scans of 36 larvae. (B-L) Whole-mount IF of *Platynereis* larvae with an antibody raised against (B) FVa, (C) RGWa, (D) FVRIa, (E) RYa, (F) PDF, (G) LEUC, (H) LUQ, (I) MIP, (J) ATO, (K) PENK, (L) FMRFa. Whole-mount scans were cropped to show only the VNC region. Antibodies label distinct neuronal tracks that span the length of the VNC. Scale bar: 20 µm.

To display the spatial relationships of 11 distinct IF labels, we employed image registration to a reference template of whole-body confocal scans using an established procedure (Asadulina et al., 2012). High-accuracy image registration of different specimens is possible in *Platynereis*, due to the stereotypic anatomy and neuronal connectivity of the larvae (Asadulina et al., 2012; Randel et al., 2015; Tomer et al., 2010). For optimal VNC registration, we generated an unbiased average whole-body reference template based on the non-rigid registration of the acetylated tubulin IF signal from 36 specimens. We aligned whole-body confocal scans of IF specimens to this reference using non-rigid image registration (Figure 4A, B; Video 1). We then took virtual cross sections from this registered dataset to analyze the spatial relationships of distinct peptidergic axons (Figure 4C-E). The arrangement of peptidergic axons in the VNC reconstructed by IF and image registration was similar to that of the VNC reconstructed by siGOLD (Figure 4F-H). To allow a more direct comparison of the spatial relationship of peptidergic axons, we performed double IF with the RGWa, PDF, and LEUC antibodies generated in rabbits and the FVa antibody generated in rats. The spatial relationships of the neurites labeled with the RGWa, PDF, and LEUC antibodies relative to six prominent FVa neurites was very similar between IF and siGOLD (Figure 4I, J). We could also detect the coexpression of FVa and PDF in some axons, both by double-IF and siGOLD. The high specificity of immunoEM, the reproducibility of labeling across sections, and the spatial correspondence of the labels between siGOLD and whole-mount IF indicate that we could accurately identify several peptidergic neurites in a serial EM dataset.

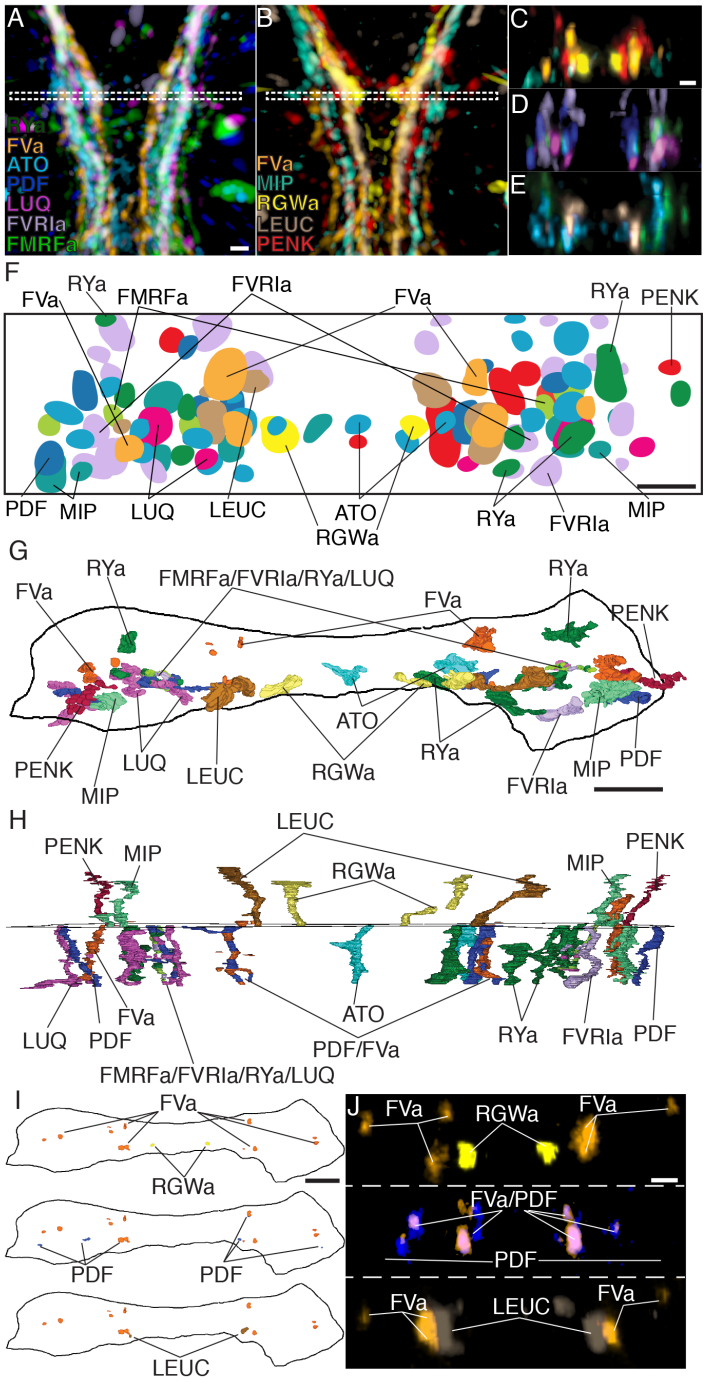

Figure 4. Axonal arrangements in the VNC detected by whole-body IF spatially match those detected by siGOLD.

(A, B) Ventral overview of individual registered full-body IF with antibodies raised against 11 different neuropeptides (colors). Image is cropped to show only the upper VNC. White dashed box indicates site where a 5 µm virtual apical cross-section in (C-E) was taken. (C-E) 5 µm virtual cross-section of individual registered full-body IFs from (A, B) in anterior view to indicate their spatial position in the VNC relative to each other. (C) RGWa, FVa, PENK, MIP, (D) FVRIa, PDF, LUQ, FMRFa (E) RYa, LEUC, ATO. (F) Schematic overview of (C-E) indicating relative positioning of individual registered antibody stainings in the VNC, anterior view. (G, H) Reconstruction of neurites labeled by siGOLD with antibodies raised against 11 different neuropeptides in the VNC of specimen HT9-5, (G) anterior view, (H) ventral view. For comparison with registered IF labeling in (A-F). (I) Single layer cross-section of siGOLD labeling in specimen HT9-5 showing neurites labeled with FVa and RGWa antibodies (top), FVa and PDF antibodies (middle), and FVa and LEUC antibodies (bottom). For comparison with double-IF in (J). (J) 2 µm virtual anterior cross-sections of the VNC of 72 hpf *Platynereis* larvae double-stained with an antibody raised against FVa (orange) and an antibody raised against RGWa (yellow, top), PDF (blue, middle) or LEUC (brown, bottom) confirm relative positioning of specific neurites in the VNC. Scale bars: (A-E) 15 µm, (F - J) 5 µm.

Application of siGOLD to a whole-body connectome dataset

Next, we tested siGOLD on a whole-body EM series of 5056 sections encompassing an entire 72 hpf *Platynereis* larva (specimen HT9-4)(Randel et al., 2015). During sectioning of this larva, we set aside series of 1 to 6 sections for later immunoEM.
In the full-body series, we used 11 antibodies to label a total of 154 sections distributed along the length of the larva (Figure 5A). We used at least two grids for each antibody, separated by up to 1,000 sections. Gold labeling in a whole-body context allowed us to identify several strongly labeled neurite profiles throughout the body. It is worth noting that sections were successfully gold labeled up to 3 years after sectioning the specimen, demonstrating the long-term stability of neuropeptide antigens in Epon sections.

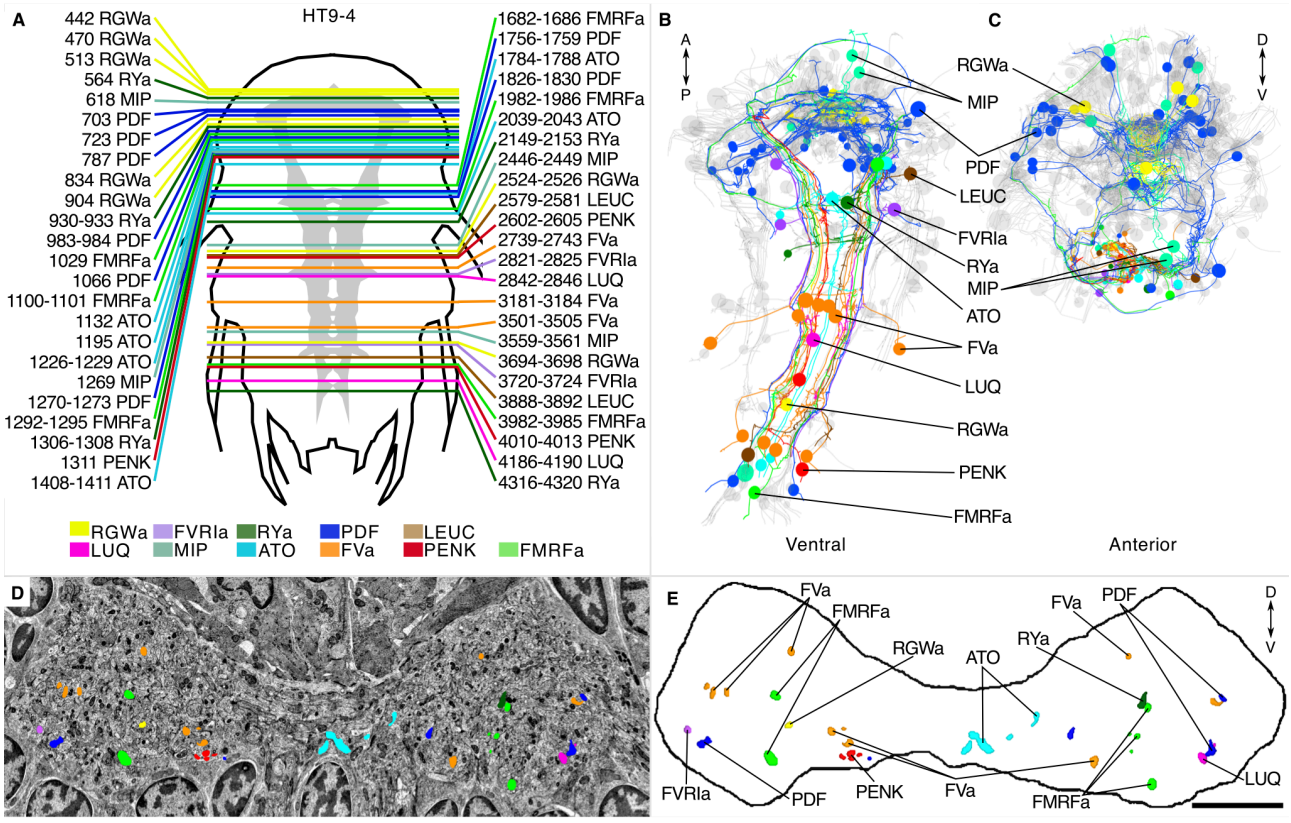

Figure 5. siGOLD labeling in a whole-body EM dataset
(A) Schematic of the HT9-4 specimen showing the position of the VNC (grey), ventral view. The entire larva was fully sectioned and imaged. Colored lines indicate the position of sections that were used for immunolabeling. For each line, layer number(s) followed by the name of the neuropeptide that was immunogold-labeled in those layers are indicated. (B, C) Ventral (B) and anterior (C) views of all fully traced immunogold-labeled peptidergic neurons. (D, E) Micrograph (D) and segmented reconstruction (E) of the cross-sections through the VNC, near the base of the circumesophageal connective at the first commissure, showing the spatial positions of all traced neuropeptidergic axons. Scale bar: (E) 5 µm.

We identified and traced 83 neurons (67 of them with a soma; Figure 5B, C; Video 2) with different peptidergic identities. We mapped the distribution of peptidergic axons crossing a section in the 1st trunk segment in a position comparable to that of HT9-5 and found similar patterns across both siGOLD-labeled larvae and the IF samples (Figure 5D, E; compare to Figure 4). For selected neurons, we quantified the number of gold particles in every immunolabeled section in HT9-4

(Figure 6). These counts again demonstrated that we could repeatedly label the same neurons in different sections, often spaced several hundred sections apart.
The reconstruction of several neurons in the whole-body serial EM dataset allowed us to further test the specificity of the immunogold labels by comparing the morphology and position of reconstructed neurons to neurons that were identified by whole-body IF. We found comparable cellular morphologies and positions for six FVa, several PDF, four MIP, and two RGWa neurons between siGOLD and IF (Figure 6). This close anatomical correspondence further supports the specificity of siGOLD and demonstrates that the method can be used to unambiguously tag fully reconstructed neurons in serial EM.

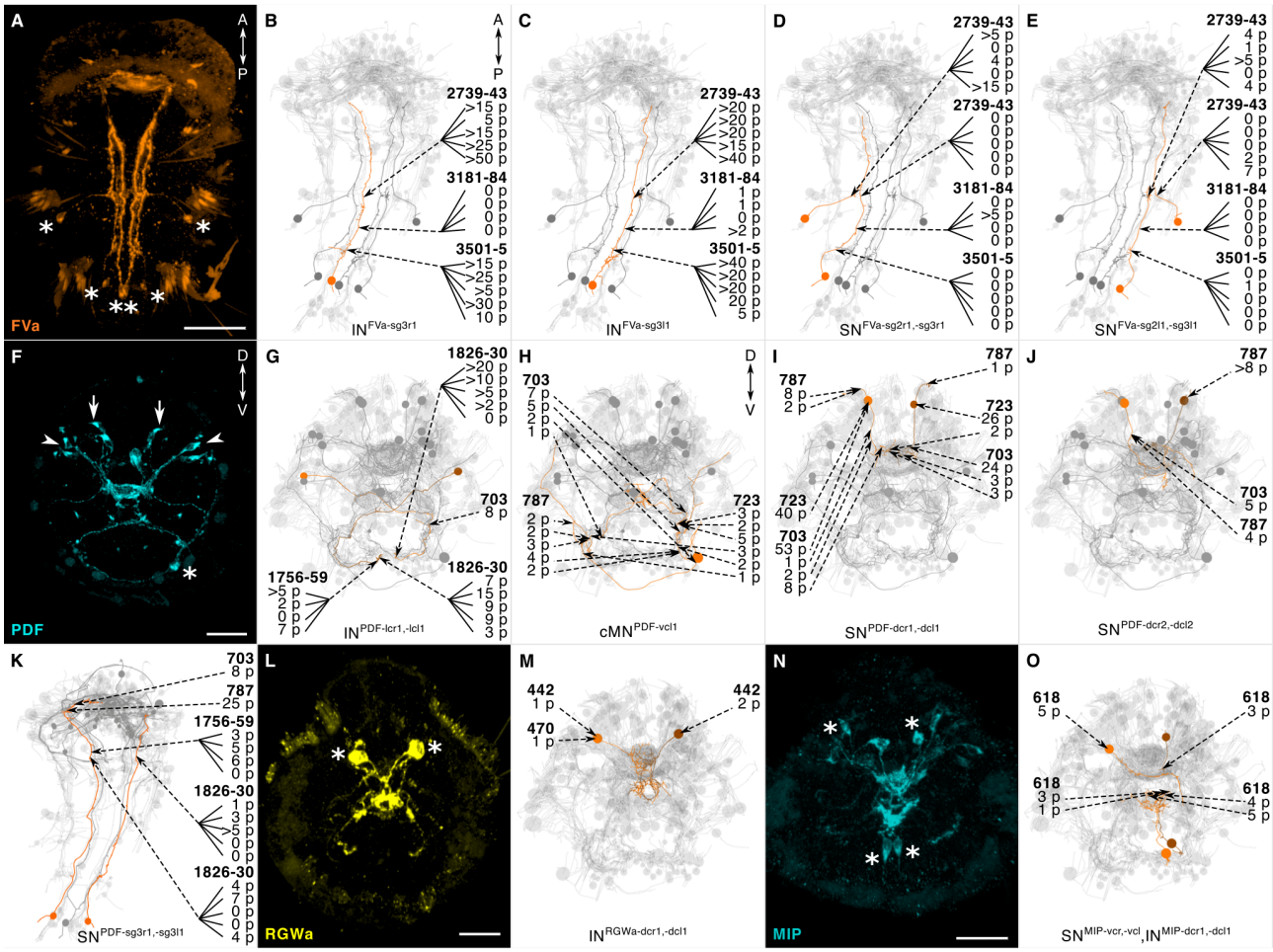

Figure 6. siGOLD labeling and whole-body neuron reconstructions
(A, F, L, N) Full body immunofluorescent labeling of FVa, PDF, RGWa, and MIP positive cells, anterior view. Note that (F) is 48 hpf, others are 72 hpf. (B-E, G-J, K, M, O) Traced neurons, identified using the siGOLD method in the full body HT9-4 project. Dashed arrows indicate immunogold labeled layers along the neurite, layer number(s) and number of gold particles per layer are shown. Traced siGOLD FVa (B-E), PDF (G-K), RGWa (M), and MIP (O) positive cells. Scale bars: (A) 50 µm; (F, L, N) 30 µm.

Connectome reconstruction of a siGOLD-labeled peptidergic circuit

The whole-body serial EM dataset combined with siGOLD labeling allows the reconstruction of circuits of neurons with specific peptidergic identities. To demonstrate this, we focused on sensory neurons in the *Platynereis* larval head that were strongly labeled by the PDF antibody. We found several sensory cells of the nuchal organs labeled with the PDF antibody (Figure 7A). The nuchal organ is a paired putative chemosensory organ in the annelid prostomium with neurons that have sensory dendrites in an olfactory pit, covered by cuticle and a patch of motile cilia (Figure 7A, B; Video 3)(Purschke, 2005). Of 30 traced nuchal organ sensory neurons (SN^{nuch}), 15 were labeled

with PDF, with some of the neurons showing strong gold labeling in multiple sections (Figure 7C). This is consistent with the labeling of the nuchal organ with the PDF antibody in IF (Figure 6F). We fully traced these PDF-positive sensory neurons and identified their direct postsynaptic targets. We found that the most strongly connected neurons, receiving up to 25 synapses from SN^{nuch} cells, were a pair of interneurons (IN^{nuch}) with a unique biramous morphology (Figure 7D-F). Additionally, we found connections to two interneurons ($IN^{RGWa\text{-}dcr1,\ \text{-}dcl1}$) that were identified by siGOLD labeling to express the RGWa neuropeptide. The SN^{nuch} cells also connected to the previously described arc interneurons (IN^{arc})(Figure 7D-F; Video 4) that are postsynaptic to the eyespot and have connections to the ventral motorneurons (Randel et al., 2015). This represents a potential functional path linking the nuchal organs to the locomotor apparatus.

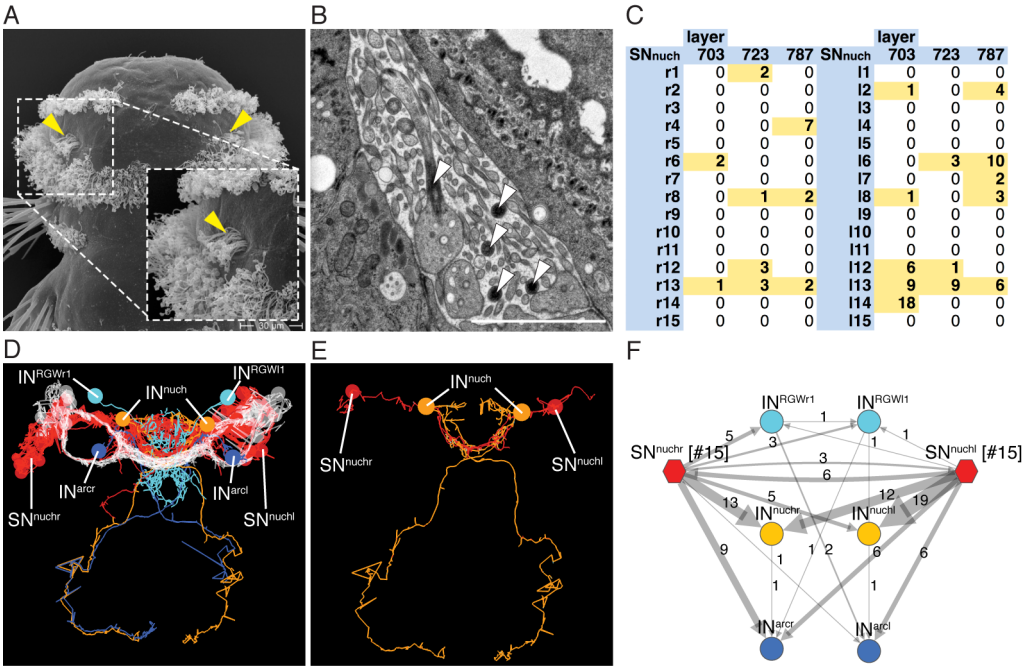

SNnuch	layer 703	723	787	SNnuch	layer 703	723	787
r1	0	2	0	l1	0	0	0
r2	0	0	0	l2	1	0	4
r3	0	0	0	l3	0	0	0
r4	0	0	7	l4	0	0	0
r5	0	0	0	l5	0	0	0
r6	2	0	0	l6	0	3	10
r7	0	0	0	l7	0	0	2
r8	0	1	2	l8	1	0	3
r9	0	0	0	l9	0	0	0
r10	0	0	0	l10	0	0	0
r11	0	0	0	l11	0	0	0
r12	0	3	0	l12	6	1	0
r13	1	3	2	l13	9	9	6
r14	0	0	0	l14	18	0	0
r15	0	0	0	l15	0	0	0

Figure 7. Reconstruction of a siGOLD-labeled peptidergic circuit
(A) SEM image of the nuchal organs (yellow arrowhead) in the dorsal-posterior head of a 72 hpf *Platynereis* larva, dorsal view. (B) TEM image of the nuchal organ showing the olfactory pit with the sensory neurons and microvilli. Arrowheads point at sensory cilia. (C) Number of gold particles identified in three different immunogold layers labeled with the PDF antibody in all SN^{nuch} sensory neurons that were fully traced. (D) 3D reconstruction of the nuchal organ circuit. SN^{nuch} sensory neurons (red), IN^{nuch} (orange), IN^{RGW} (cyan), and IN^{arc} (blue) interneurons are shown. The photoreceptor cells of the adult eyes are shown in white as a reference. (E) 3D reconstruction of two SN^{nuch} sensory neurons (red) and the two IN^{nuch} (orange) that represent the major synaptic targets of the sensory neurons. (F) Graph representation of the nuchal organ circuit. Nodes represent neurons or groups of neurons, edges represent synaptic connections. The number of synapses is indicated on each arrow. Edge thickness is proportional to the number of synapses. Scale bar: (A) 30 µm; (B) 1 µm.

DISCUSSION

In this paper we introduced siGOLD, a method to identify distinct peptidergic neurons in large serial EM datasets in combination with whole-body connectome reconstruction. Our method uses Epon embedding to allow robust sectioning of thousands of sections and to provide high ultrastructural detail. We take advantage of the unique properties of neuropeptide antigens, including their small size, abundance, and concentration in dense-core vesicles. In addition, neuropeptides are often amidated, conferring increased stability and high immunogenicity to the mature peptides (Conzelmann and Jékely, 2012; Eipper et al., 1992). We demonstrated the extreme

longevity of neuropeptide immunoreactivity by performing immunoEM of 'set-aside' layers years after sectioning and the acquisition of the complete image series had been completed.
Neuropeptides have the additional benefit of being distributed along the entire length of the axon, due to their active circulation throughout the axon (Wong et al., 2012). This allowed us to identify neurons based on only a few immunolabeled sections throughout each neuron's axon. This sparse labeling approach allows the application of several different antibody markers to identify distinct neurons in different sets of sections, and is also applicable to very large, even full-body EM datasets. siGOLD is in principle also compatible with the high-throughput automatic tape-collecting ultramicrotome (ATUM) method (Hayworth et al., 2014), but not with the serial block-face method (Denk and Horstmann, 2004).
Our siGOLD method differs from array tomography in that we do not attempt to stain every section with multiple markers, but rather use one marker per section on sparsely distributed sections. siGOLD relies on direct immunoEM of sections and does not rely on registering EM and IF images to assign immunolabels to specific structures. With siGOLD we enjoy the full resolving power of the electron microscope, and could also identify individual dense-core vesicles that carry strong immunogold signal.
We also demonstrated that siGOLD labeling can be used to assign peptidergic identities to neurons in serial sections derived from large tissue blocks, in conjunction with the reconstruction of the synaptic connectivity of these neurons. We reconstructed the partial circuitry of the nuchal organs, representing a candidate chemotactic circuit in the 72 hpf *Platynereis* larval head. The sensory neurons of the nuchal organ express the PDF neuropeptide, suggesting peptidergic transmission to the target interneurons. One type of postsynaptic interneuron expresses the RGWa neuropeptide, indicating a strong peptidergic character of the circuit.
The mapping of peptidergic neurons by siGOLD, together with the recent identification of several neuropeptide receptors in *Platynereis* (Bauknecht and Jékely, 2015), open up the possibility of a cellular-level analysis of peptidergic neurotransmission in diverse circuits in *Platynereis*. In total, we have identified 83 different peptidergic neurons out of approximately 2000 total in the *Platynereis* whole-body dataset. Further connectome tracing in these data will provide a rich source of information about specific peptidergic circuit motifs in this animal.
In *Platynereis*, as well as humans, *C. elegans*, and *Drosophila*, the majority of mature neuropeptides are amidated (Jékely, 2013; Mirabeau and Joly, 2013), and several antibodies are available. Furthermore, most neuropeptides are expressed in small subsets of specific neurons, providing ideal markers for the identification of multiple neuron types. Our siGOLD approach and the use of neuropeptide antibodies could be adapted to enrich connectome data with molecular information also in other organisms. The direct overlaying of chemical neuromodulatory maps onto synaptic connectomic maps by siGOLD opens up new possibilities for the study of nervous systems.

Acknowledgments
We thank Matthias Flötenmeyer and Heinz Schwarz for advice on immunogold labeling and EM, Nadine Randel for help with tracing, Stephan Saalfeld for advice on the generation of an unbiased template for image registration, David Mastronarde for developing serialEM, Steffen Schmidt for maintaining our Catmaid server, Aurora Panzera for help with microinjections, and Dorothee Hildebrandt for animal care. The research leading to these results received funding from the European Research Council under the European Union's Seventh Framework Programme (FP7/2007-2013)/European Research Council Grant Agreement 260821. This project is supported by the Marie Curie ITN "Neptune", GA 317172, funded under the FP7, PEOPLE Work Programme of the European Commission.

EXPERIMENTAL PROCEDURES

Transmission electron microscopy

Fixation and embedding was carried out on 72 hpf *Platynereis* larvae (HT9-4 and HT9-5) as described previously (Conzelmann et al., 2013). 40 nm serial sections were cut on a Reichert Jung Ultracut E microtome using a 45º DiATOME Diamond knife. The sections were collected on single-slotted copper grids (NOTCH-NUM 2_1 mm, Science Service, Munich) with Formvar support film. For the HT9-5 serial sections, the samples were collected on single-slotted nickel grids coated with Formvar support film. The ribbons of sections were picked up from underneath and on the under-side (the notch side) of the grids. This method allowed the section ribbons to stay afloat and stretch while being dried in the oven, eliminating most wrinkles from the sections. The section statistics for the HT9-4 specimen (or NAOMI) were previously described (Randel et al., 2015) and an updated table with the immunoEM information is shown in Supplementary table 1. For HT9-5, 200 sections were cut from the VNC (first segment) and imaged for tracing, segmentation and analysis.

Grid handling

To meet the demand for consistent section processing in large-scale serial reconstruction projects, we have developed an effective method of grid handling based on a method first described by Rowley and Moran (Rowley and Moran, 1975). The following method has proven safe for contrast staining, immunolabeling, and carbon coating. It stabilizes the grids during the staining procedures and saves time by eliminating the need for one-by-one grid manipulation.
A 6x12 hole microwell mini tray plate (NUNC™ Brand MicroWell® Mini Trays) was cut into two 3x12 hole plate strips. Holes were drilled through each of the plate's micro-cups using a fine drill to later allow the plastic support film to dry evenly on both sides. Plates were rinsed with 75% ethanol, followed by distilled water, then sonicated to eliminate dust and burr particles. This procedure produced two lightweight plates similar to that described by Rowley and Moran (Rowley and Moran, 1975) with the additional benefit of 'raised', separated walls. This approach minimizes cross-contamination by diffusion of solutions during the staining and labeling procedures. A strip of Formvar support film was used to coat the microwell mini plate on the topside of the plate. A small water droplet (10 µl) was placed on each hole of the plate on the support film using a filtered syringe. A grid containing previously cut sections was placed (sections facing up) on each droplet and dried in the 50ºC oven until the grids and the plastic support film had fused. Grids were then ready for immunolabeling and contrast staining by inverting and matching to the micro-cups of a full mini tray with desired solutions (Figure 1A – Mini tray).

Contrasting

Dried sections were contrast stained with drops of 2% aqueous uranyl acetate for 6 min. Grids were washed by gently lowering the entire plate into a clean glass beaker of filtered distilled water. Excess water was wicked away with filter paper and the grids were dried at 50 ºC for 1-2 min. Next, the grids were stained with drops of Sato's triple lead stain (Hanaichi et al., 1986) for 4 min. Grids were washed and dried as described above and dried at 50 ºC for 1 min. Grids were then carbon coated before being imaged with a FEI TECNAI Spirit electron microscope.

Immunogold silver-enhancement method

For immunoEM, we have eliminated the etching step prior to primary antibody incubation. We have observed that the treatment with the etching solution destroys ultrastructural integrity. In our technique, the use of sheep serum and bovine serum albumin mixed with Tween-20 at pH of 7.9 greatly enhanced the immunogold signal.

The following protocol was performed over a one-day period and is an optimized version of a protocol by Stierhof (Stierhof et al., 1991) for Epon-embedded sections. All incubations up to the silver enhancement point were done in the TBST-BGN (Tris buffer saline with Tween-20, BSA, Fish Gelatin and Normal Sheep Serum, pH 7.9; see section below on preparing the buffer). First, sections were blocked with TBST-BGN for 10 minutes; blocked sections were then incubated with primary antibody (1:25 dilution) in TBST-BGN for 2 hours. Grids were washed twice with TBST-BGN for 5 minutes, and then incubated with secondary goat anti-rabbit IgG antibody with gold conjugates (AURION Ultra Small Immunogold Reagents; size 0.8 nm) at 1:50 dilution for 1 hour. Grids were then washed with TBST-BGN twice for 5 minutes, then washed twice with filtered distilled water for 5 minutes, followed by fixation with 1% glutaraldehyde in filtered distilled water for 5 min. Sections were washed in filtered distilled water twice for 5 min. Silver enhancement was applied with Aurion silver-enhancement kit for up to 47 minutes. The time interval of silver enhancement was dependent on temperature and concentration of the silver-enhancement solution. Gold size growth was approximately 15-20 nm within this time interval, a size appropriate for observation of gold particles in EM. Silver enhancement was stopped with three 3-minute washes in filtered distilled water. Excess water was gently wicked from the back of the plate and individual holes with wedges of Whatman filter paper. Grids were dried in a 50 ºC oven and then contrasted (see above).

Preparation of blocking and wash buffer solution

Buffer concentration and consistency is very important in immunological reactions. We compared many protocols to achieve the best buffer for our experiments. We found that a saline buffer with Tris, Tween, bovine serum albumin (BSA), fish Gelatin, and normal serum (TBST-BGN), worked well. Our solutions were always freshly prepared on the day of the experiment. To prepare the buffer for immunoEM, three separate solutions were made: (1) 0.61 g Trizma, 0.90 g NaCl, and 70 ml of distilled water, (2) 1.0 g of BSA, 1.5 ml normal sheep serum, 500 µl Tween-20, and 20 ml distilled water, and (3) 0.01g of fish Gelatin and 10 ml of distilled water. Solution 3 was heated to dissolve and then cooled before being added to solution 1 and 2. Finally, solutions 1-3 were combined and gently mixed. The buffer solution was then adjusted to pH of 7.9 using 1 M HCl and syringe filtered with a 0.45 µm filter.

Imaging and post-processing

Image acquisition of TEM serial sections was performed on a FEI TECNAI Spirit transmission electron microscope equipped with an UltraScan 4000 4X4k digital camera using the image acquisition software Digital Micrograph (Gatan Software Team Inc., Pleasanton) and SerialEM (Mastronarde, 2005). The images for the HT9-4 and HT9-5 samples were scanned at a pixel resolution of 5.71 nm/pixel and 2.22 nm/pixel respectively. Image stitching and alignment were accomplished using TrakEM2 (Cardona et al., 2010; Cardona et al., 2012). All structures were segmented manually as area-lists, and exported into 3Dviewer and Blender as previously described (Asadulina et al., 2015). Tracing and annotation of the connectome were performed with CATMAID, a collaborative annotation toolkit for large-scale image data (Saalfeld et al., 2009).

IF and image registration

Antibodies were generated by immunizing rats or rabbits with synthetic, amidated peptides. All peptides contained an N-term Cys that was used for coupling. Antibodies were affinity purified from sera as previously described (Conzelmann and Jékely, 2012). Triple-staining with FVa rat (AF488 secondary antibody rat), other neuropeptide rabbit (AF647 secondary antibody rabbit), and acetylated-tubulin mouse (high-fidelity AF555 secondary antibody mouse) was carried out as previously described (Conzelmann and Jékely, 2012).

For image registration, an average full-body acetylated tubulin reference template was generated for 72 hpf *Platynereis* using a modification of a previously described method (Asadulina et al., 2012). We used full-body scans of 36 larvae generated on a Zeiss LSM 780 confocal microscope with ZenBlue software. All stacks were oriented and their centers of mass were aligned. Stacks were averaged and all stacks were aligned to this first average template using affine transformation. The 24 registered stacks most similar to the first average (as determined by an iteration metric) were then used to create an affine-transformed average. All original oriented stacks were then aligned to the affine-transformed average using affine and deformable transformation. The 24 registered stacks most similar to the affine-transformed average were then used to create an affine/deformable-transformed average. All original oriented stacks were then aligned to the affine/deformable-transformed average using affine and deformable transformation. The 24 registered stacks most similar to the affine/deformable-transformed average were then used to generate the final average acetylated tubulin reference template. The final average stack was unbiased, and was used for image registration.
Imaris was used for image processing (adjusting brightness and contrast uniformly) and to take virtual cross-sections of the VNC for comparison with siGOLD samples.

Morpholino injection

Morpholino injections were performed as previously described (Conzelmann et al., 2013). We used the following morpholinos to target the various neuropeptide precursor genes (GeneTools, LLC): Pdu-FMRFa-start MO CCACTGGTCCCTCATGGCAGGGTTT, Pdu-PDF-start MO CTGAACTGTCTTGCTTGATCCCATC, Pdu-ATO-start MO CACAGGACTACCTTCATTTTTCTGA, Pdu-LUQ-start MO GTATTTGCACAACATAGTGATAGTC, Pdu-PENK-start MO GAGGAGGACCACCAATATCTTCATC, Pdu-RYa-start MO TATAGACATGACACCTTGTTGGAGT, Pdu-LEUC-start2 MO TCTTGGCTGAACTCATTGCGGCC, Pdu-FVa-start MO CCATCCGCCCACGCTCATATGCATC, Pdu-FVRIa-start MO CCCCCTTCATACTGTCACAACGGAC, Pdu-RGWa-start MO CGACGACCCCCTGTAGCTTCATGTC.

REFERENCES

Asadulina, A., Panzera, A., Verasztó, C., Liebig, C. and Jékely, G. (2012). Whole-body gene expression pattern registration in Platynereis larvae. *Evodevo* **3**, 27.

Asadulina, A., Conzelmann, M., Williams, E. A., Panzera, A. and Jékely, G. (2015). Object-based representation and analysis of light and electron microscopic volume data using Blender. *BMC Bioinformatics* **16**, 229.

Bargmann, C. I. (2012). Beyond the connectome: how neuromodulators shape neural circuits. *Bioessays* **34**, 458–465.

Bargmann, C. I. and Marder, E. (2013). From the connectome to brain function. *Nat Methods* **10**, 483–490.

Bauknecht, P. and Jékely, G. (2015). Large-Scale Combinatorial Deorphanization of Platynereis Neuropeptide GPCRs. *Cell Rep*.

Bock, D. D., Lee, W. C., Kerlin, A. M., Andermann, M. L., Hood, G., Wetzel, A. W., Yurgenson, S., Soucy, E. R., Kim, H. S. and Reid, R. C. (2011). Network anatomy and in vivo physiology of visual cortical neurons. *Nature* **471**, 177–182.

Briggman, K. L., Helmstaedter, M. and Denk, W. (2011). Wiring specificity in the direction-selectivity circuit of the retina. *Nature* **471**, 183–188.

Brorson, S. H. (1998). Comparison of the immunogold labeling of single light chains and whole immunoglobulins with anti-kappa on LR-white and epoxy sections. *Micron* **29**, 439–443.

Brorson, S. H. and Reinholt, F. P. (2008). The intensity of immunogold labeling of deplasticized acrylic sections compared to deplasticized epoxy sections-Theoretical deductions and experimental data. *Micron* **39**, 144–150.

Bucher, D. and Marder, E. (2013). SnapShot: Neuromodulation. *Cell* **155**, 482–482.e1.

Bumbarger, D. J., Riebesell, M., Rödelsperger, C. and Sommer, R. J. (2013). System-wide rewiring underlies behavioral differences in predatory and bacterial-feeding nematodes. *Cell* **152**, 109–119.

Cardona, A., Saalfeld, S., Preibisch, S., Schmid, B., Cheng, A., Pulokas, J., Tomancak, P. and Hartenstein, V. (2010). An integrated micro- and macroarchitectural analysis of the Drosophila brain by computer-assisted serial section electron microscopy. *PLoS Biol* **8**,.

Cardona, A., Saalfeld, S., Schindelin, J., Arganda-Carreras, I., Preibisch, S., Longair, M., Tomancak, P., Hartenstein, V. and Douglas, R. J. (2012). TrakEM2 software for neural circuit reconstruction. *PLoS ONE* **7**, e38011.

Collman, F., Buchanan, J., Phend, K. D., Micheva, K. D., Weinberg, R. J. and Smith, S. J. (2015). Mapping synapses by conjugate light-electron array tomography. *J Neurosci* **35**, 5792–5807.

Conzelmann, M. and Jékely, G. (2012). Antibodies against conserved amidated neuropeptide epitopes enrich the comparative neurobiology toolbox. *Evodevo* **3**, 23.

Conzelmann, M., Williams, E. A., Tunaru, S., Randel, N., Shahidi, R., Asadulina, A., Berger, J., Offermanns, S. and Jékely, G. (2013). Conserved MIP receptor-ligand pair regulates Platynereis larval settlement. *Proc Natl Acad Sci U S A* **110**, 8224–8229.

De Paul, A., H., J., P., J., Gutirrez, S., A., A., A., C. and I., A. (2012). Immunoelectron Microscopy: A Reliable Tool for the Analysis of Cellular Processes. In *Applications of Immunocytochemistry* (ed. Dehghani, H.), InTech.

Denk, W. and Horstmann, H. (2004). Serial block-face scanning electron microscopy to reconstruct three-dimensional tissue nanostructure. *PLoS Biol* **2**, e329.

Eipper, B. A., Stoffers, D. A. and Mains, R. E. (1992). The biosynthesis of neuropeptides: peptide alpha-amidation. *Annu Rev Neurosci* **15**, 57–85.

Hanaichi, T., Sato, T., Iwamoto, T., Malavasi-Yamashiro, J., Hoshino, M. and Mizuno, N. (1986). A Stable Lead by Modification of Sato Method. *Journal of Electron Microscopy* **35**, 304–306.

Hayworth, K. J., Morgan, J. L., Schalek, R., Berger, D. R., Hildebrand, D. G. and Lichtman, J. W. (2014). Imaging ATUM ultrathin section libraries with WaferMapper: a multi-scale approach to EM reconstruction of neural circuits. *Front Neural Circuits* **8**, 68.

Jékely, G. (2013). Global view of the evolution and diversity of metazoan neuropeptide signaling. *Proc Natl Acad Sci U S A* **110**, 8702–8707.

Lin, T. Y., Luo, J., Shinomiya, K., Ting, C. Y., Lu, Z., Meinerzhagen, I. A. and Lee, C. H. (2015). Mapping chromatic pathways in the Drosophila visual system. *J Comp Neurol*.

Marder, E. (2012). Neuromodulation of neuronal circuits: back to the future. *Neuron* **76**, 1–11.

Martell, J. D., Deerinck, T. J., Sancak, Y., Poulos, T. L., Mootha, V. K., Sosinsky, G. E., Ellisman, M. H. and Ting, A. Y. (2012). Engineered ascorbate peroxidase as a genetically encoded reporter for electron microscopy. *Nat Biotechnol* **30**, 1143–1148.

Mastronarde, D. N. (2005). Automated electron microscope tomography using robust prediction of specimen movements. *J Struct Biol* **152**, 36–51.

Micheva, K. D. and Smith, S. J. (2007). Array tomography: a new tool for imaging the molecular architecture and ultrastructure of neural circuits. *Neuron* **55**, 25–36.

Mirabeau, O. and Joly, J. S. (2013). Molecular evolution of peptidergic signaling systems in bilaterians. *Proc Natl Acad Sci U S A* **110**, E2028–E2037.

Morgan, J. L. and Lichtman, J. W. (2013). Why not connectomics? *Nat Methods* **10**, 494–500.

Ohyama, T., Schneider-Mizell, C. M., Fetter, R. D., Aleman, J. V., Franconville, R., Rivera-Alba, M., Mensh, B. D., Branson, K. M., Simpson, J. H., Truman, J. W., et al. (2015). A multilevel multimodal circuit enhances action selection in Drosophila. *Nature* **520**, 633–639.

Purschke, G. (2005). Sense organs in polychaetes (Annelida). *Hydrobiologia* **535**, 53–78.

Randel, N., Asadulina, A., Bezares-Calderón, L. A., Verasztó, C., Williams, E. A., Conzelmann, M., Shahidi, R. and Jékely, G. (2014). Neuronal connectome of a sensory-motor circuit for visual navigation. *elife* **3**,.

Randel, N., Shahidi, R., Verasztó, C., Bezares-Calderón, L. A., Schmidt, S. and Jékely, G. (2015). Inter-individual stereotypy of the Platynereis larval visual connectome. *elife* **4**,.

Rowley, J. and Moran, D. (1975). A simple procedure for mounting wrinkle-free sections on formvar-coated slot grids. *Ultramicroscopy* **1**, 151–155.

Saalfeld, S., Cardona, A., Hartenstein, V. and Tomancak, P. (2009). CATMAID: collaborative annotation toolkit for massive amounts of image data. *Bioinformatics* **25**, 1984–1986.

Shu, X., Lev-Ram, V., Deerinck, T. J., Qi, Y., Ramko, E. B., Davidson, M. W., Jin, Y., Ellisman, M. H. and Tsien, R. Y. (2011). A genetically encoded tag for correlated light and electron microscopy of intact cells, tissues, and organisms. *PLoS Biol* **9**, e1001041.

Stierhof, Y., Humbel, B. and Schwarz, H. (1991). Suitability of different silver enhancement methods applied to 1 nm colloidal gold particles: An immunoelectron microscopic study. *J Electron Microsc Tech* **17**, 336–343.

Tomer, R., Denes, A. S., Tessmar-Raible, K. and Arendt, D. (2010). Profiling by image registration reveals common origin of annelid mushroom bodies and vertebrate pallium. *Cell* **142**, 800–809.

Tosches, M. A., Bucher, D., Vopalensky, P. and Arendt, D. (2014). Melatonin signaling controls circadian swimming behavior in marine zooplankton. *Cell* **159**, 46–57.

Viswanathan, S., Williams, M. E., Bloss, E. B., Stasevich, T. J., Speer, C. M., Nern, A., Pfeiffer, B. D., Hooks, B. M., Li, W. P., English, B. P., et al. (2015). High-performance probes for light and electron microscopy. *Nat Methods* **12**, 568–576.

White, J. G., Southgate, E., Thomson, J. N. and Brenner, S. (1986). The structure of the nervous system of the nematode Caenorhabditis elegans. *Philos Trans R Soc Lond, B, Biol Sci* **314**, 1–340.

Williams, E. A., Conzelmann, M. and Jékely, G. (2015). Myoinhibitory peptide regulates feeding in the marine annelid Platynereis. *Front Zool* **12**, 1.

Wong, M. Y., Zhou, C., Shakiryanova, D., Lloyd, T. E., Deitcher, D. L. and Levitan, E. S. (2012). Neuropeptide delivery to synapses by long-range vesicle circulation and sporadic capture. *Cell* **148**, 1029–1038.

Zupanc, G. (1996). Peptidergic transmission: From morphological correlates to functional implications. *Micron* **27**, 35–91.

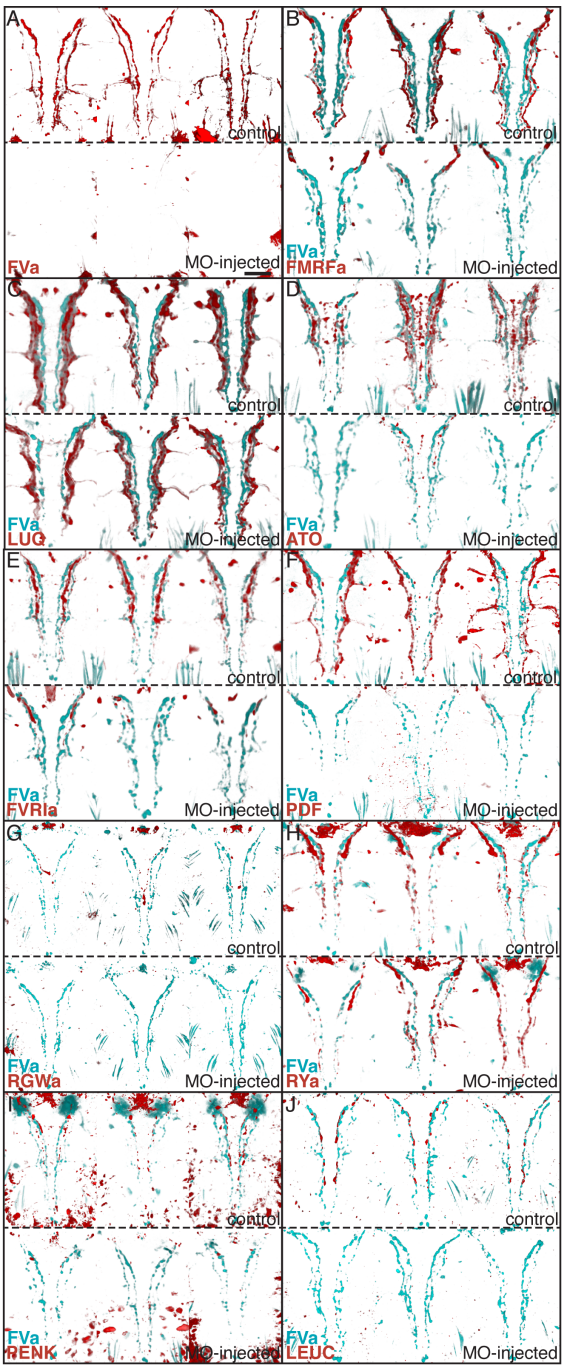

Supplementary figure 1. Morpholino-mediated knockdown of proneuropeptides followed by whole-mount IF indicates antibody specificities.

Whole-mount IF of 72 hpf uninjected control *Platynereis* larvae and larvae micro-injected with translation-blocking morpholinos (MOs) targeting different neuropeptide precursor genes. FVa-knockdown and control larvae were stained with an antibody raised against FVa and counterstained with acetylated tubulin. All other control and knockdown larvae were co-stained with an antibody raised against FVa and an antibody raised against the MO target peptide indicated and counterstained with acetylated tubulin. All larvae are shown in ventral view. For each neuropeptide, three control larvae (top) and three MO-knockdown larvae (bottom) are shown. (A) FVa knockdown and control larvae with antibody raised against FVa. (B) FMRFa knockdown and control larvae with antibody raised against FMRFa. (C) LUQ knockdown and control larvae with antibody raised against LUQ. (D) ATO knockdown and control larvae with antibody raised against ATO. (E) FVRIa knockdown and control larvae with antibody raised against FVRIa. (F) PDF knockdown and control larvae with antibody raised against PDF. (G) RGWa knockdown and control larvae with antibody raised against RGWa. Note that the staining in the head is eliminated following knockdown. The staining in the VNC was too weak in these samples. (H) RYa knockdown and control larvae with antibody raised against RYa. (I) PENK knockdown and control larvae with antibody raised against PENK. (J) LEUC knockdown and control larvae with antibody raised against LEUC. Scale bar: 30 µm.